

Soft Matter

Accepted Manuscript

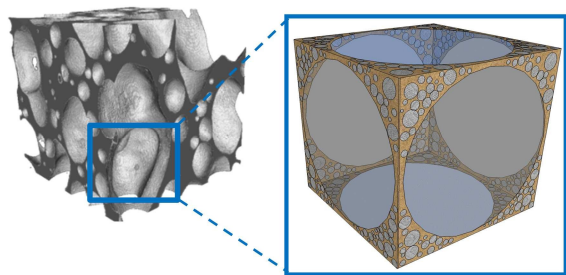


This is an *Accepted Manuscript*, which has been through the Royal Society of Chemistry peer review process and has been accepted for publication.

Accepted Manuscripts are published online shortly after acceptance, before technical editing, formatting and proof reading. Using this free service, authors can make their results available to the community, in citable form, before we publish the edited article. We will replace this *Accepted Manuscript* with the edited and formatted *Advance Article* as soon as it is available.

You can find more information about *Accepted Manuscripts* in the [Information for Authors](#).

Please note that technical editing may introduce minor changes to the text and/or graphics, which may alter content. The journal's standard [Terms & Conditions](#) and the [Ethical guidelines](#) still apply. In no event shall the Royal Society of Chemistry be held responsible for any errors or omissions in this *Accepted Manuscript* or any consequences arising from the use of any information it contains.



X-ray tomography image of fermented dough, and proposed scheme of a structure element representing gas cell with liquid films walls, embedded in the composite matrix of starch granules-gluten filaments.

Growth and setting of gas bubbles in a viscoelastic matrix imaged by X-ray microtomography: the evolution of cellular structure in fermenting wheat flour dough

A. Turbin-Orger,^a P. Babin,^{b,c} E. Boller,^d L. Chaunier,^a H. Chiron,^a G. Della Valle,^{a*} R. Dendievel,^b AL. Réguerre,^a L. Salvo^b

^a INRA, UR 1268 Biopolymères, Interactions & Assemblages (BIA), 44316 Nantes, France

^b SIMAP, UMR CNRS 5266, Grenoble Institute of Technology, 38402 St Martin d'Hères, France

^c present address: ARKEMA–CERDATO, 27470 Serquigny, France

^d ESRF, Beamline ID19, CS 40220, 38043 Grenoble Cedex 9, France

* Corresponding author: guy.della-valle@nantes.inra.fr

Address: Guy Della Valle, BP 71627, 44316 NANTES, Cédex 3, France; Phone: +33 (0)2 40 67 50 00

Abstract

X-ray tomography is a relevant technique for the dynamic follow-up of gas bubbles in an opaque viscoelastic matrix, especially using image analysis. It has been applied here to pieces of fermenting wheat flour dough of various compositions, at two different voxel sizes (15 and then 5 μm). The resulting evolutions of the main cellular features show that the creation of cellular structure follows two regimes that are defined by a characteristic time of connectivity, t_c [30, 80 min]: first ($t \leq t_c$), bubbles grow freely and then ($t \geq t_c$) they connect since the percolation of the gas phase is limited by liquid films. During the first regime, bubbles can be tracked and the local strain rate measured. Its values ($10^{-4} - 5 \cdot 10^{-4} \text{s}^{-1}$) are in agreement with those computed from dough viscosity and internal gas pressure, both of which depend on composition. For larger porosity, $P=0.64$ in our case, and thus occurring in the second regime, different cellular structures are obtained and XRT images show deformed gas cells that display complex shapes. The comparison of these images with confocal laser scanning microscopy imaging suggests the presence of liquid films that separate these cells. The dough can therefore be seen as a three-phase medium: viscoelastic matrix/gas cell/liquid phase. The contributions of the different levels of matter organization can be integrated by defining a capillary number ($Ca^* = 0.1 - 1$) that makes it possible to predict the macroscopic dough behavior.

Keywords: capillary number, connectivity, elongational viscosity, imaging, liquid phase, porosity

1. Introduction

Due to its importance for sensory and nutritional properties and to its complexity, food structure is a pertinent topic for addressing multidisciplinary scientific challenges.¹ One way to overcome this complexity is to study model foods, as proposed in the EU-project Dream,² where bread was chosen as a model for cereal foods and considered as a solid foam. As such, its properties are strongly related to its cellular structure.^{3,4} Bread cellular structure results from a chain of different operations that define the bread-making process. During the first operation - mixing flour with water - the gluten network is formed, with significant adhesion to starch granules. Both of these phenomena contribute to the rheological properties of the starch/gluten matrix and the dough.⁵ The cellular structure is then set at the end of the fermentation step after bubble growth due to CO₂ production by yeast, leading to a final porosity of approximately 70%. This structure is not particularly affected by baking, the last step, which is essential for crust creation and crumb setting as a result of gluten cross-linking and starch melting and, consequently, for bread acceptance and digestibility.

Deeper insight into gas bubble growth requires microscopic observation of this opaque medium, the wheat flour dough. Various methods used to do this, such as electronic microscopy,⁶ magnetic resonance micro-imaging⁷ and ultrasound,⁸ have the shortcomings of either being invasive, modifying the sample during preparation, having limited contrast, or being restricted to two-dimensional information. X-ray tomography (XRT), which has been applied to solid foams, is non-invasive and provides highly contrasted three-dimensional (3D) images of materials, with a voxel size of 1 μm as an order of magnitude.⁹ Due to these advantages, XRT has been applied to analyze the cellular structure of cereal food foams.¹⁰ It has also recently been used to analyze ice cream as a three-phase medium under cyclic temperature changes.¹¹ Due to high-density contrast, XRT is particularly well suited for studying the phenomena involved in the creation of the cellular structure of wheat flour dough. This cellular structure is initiated at the end of mixing, like the growth of gas bubbles in the starch/gluten matrix, whose density is approximately $1.25 \cdot 10^3 \text{ kg/m}^3$.¹² However, in the case of dynamic imaging, a compromise has to be found between spatial and time resolutions so that images can be acquired fast enough compared to the structural changes studied. For this purpose, synchrotron radiation is a good option.

We analyzed the bubble growth and foam setting of a lean dough composition during bread making using XRT at the European Synchrotron Radiation Facility (ESRF), with a voxel size of 15 μm and a time acquisition of 30 s. Results suggested that the development of

gas cells could first be governed by simple bubble growth in a viscous matrix and, second, that bubbles become connected and coalesce.¹³ Concerning the second step, we studied different dough compositions, and using XRT with a voxel size of 5 μm , we were able to show that different cellular structures are obtained for the same porosity value.¹⁴ Clearly, the underlying mechanisms that govern these two steps must be identified, requiring image analysis. At the same time, other techniques such as microscopy and rheology can provide useful information. Confocal scanning laser microscopy (CSLM) can be used to localize the components, close to the gas bubbles, to determine the role of tensioactive agents.¹⁵ At the macroscopic scale, the expansion of dough during fermentation can be assessed by 2D imaging.¹⁶ The elongational properties of the starch/gluten matrix play an essential part in the development of gas cell structure during dough fermentation¹⁷ and can be measured by uniaxial compression under lubricated conditions.¹⁸ The results obtained from these various techniques could be combined to link the different levels of organization of wheat flour dough and explain its macroscopic behavior.

In this paper, we applied X-ray tomography to the follow-up of the evolution of cellular structure in fermenting wheat flour dough, firstly, in order to identify the mechanisms of gas bubble growth in a viscoelastic opaque medium and, secondly, to determine the phenomena that limit their coalescence and that stabilize the cellular structure. To do this, we extended the dough composition previously studied to the domain where the resulting baked dough, *i.e.*, “the bread” is porous enough to be considered as a solid foam.² We then followed the development of the cellular structure from the beginning to the end of dough fermentation, with a voxel size of 15 μm . Using a higher resolution (voxel size: 5 μm), we subsequently focused on the last stage of fermentation with a larger porosity, when bubbles are connected and possibly coalesce, in order to propose a schematic view of an elementary dough volume organization. Finally, by comparing these results with those obtained by CSLM in this paper, and also with results on dough rheology and macroscopic scale behavior from former studies, we defined an apparent capillary number that may be used to control dough macroscopic behavior.

2. Materials and methods

Two series of micro-tomography experiments were carried out at the European Synchrotron Radiation Facility (ESRF, Grenoble). The first one, on beamline BM05, with a voxel size of

15 μm , covered the whole fermentation operation, and the second one, performed on beamline ID19, with a voxel size of 5 μm , focused on the later stage of fermentation.

2.1 Dough sample preparation

Dough pieces were prepared from wheat flour (Giraudineau, Saint Colombar; protein: 10.5%; moisture content: 15%; ash: 0.55%) according to different compositions as reported in Table 1. Up to 3% of fresh yeast was added during mixing, and only 2% in the second series in order to slow down the phenomena and better focus on bubble interactions. Wheat flour, water and other ingredients were mixed in a VMI oblique axis mixer (Montaigu) with a first mixing step at 100 rpm for 4 min and a texturing step at 200 rpm for 8 min. The dough temperature at the end of mixing was $25\pm 1^\circ\text{C}$. The compositions were selected in the following range (g/100 g wheat flour): $55 \leq \text{water} \leq 66$; $0 \leq \text{sugar} \leq 15$; and $0 \leq \text{fat} \leq 10$, which led to an interval of the liquid volume fraction of $0.58 \leq \Phi_{vl} \leq 0.63$, assuming that sugar was solubilized in water. In this domain, model doughs were previously tested for their sensory (texture) and nutritional properties. It was observed that outside of these ranges, i.e., excessively high concentrations of fat or sugar, the baked product was too dense and did not lead to an aerated cellular structure.²

2.2 Microtomography experiments

The X-ray beam produced at the synchrotron ESRF (Grenoble) has properties that make it possible to obtain both absorption and contrast of material with an optimized signal-to-noise ratio. The main properties are the coherence and the high intensity flux of the beam. This technique has made it possible to distinguish between the starch/gluten matrix and the gas cells within the fermented dough.¹³ The fast X-ray tomography experiments were performed on beam line BM05, at a beam energy of 18 keV and with an exposure time for a single radiograph of 20 ms. In these conditions, a scan of 400 radiographs over 180 degrees took less than 30 s.

In addition to this initial technique, we used the ID19 beamline in order to detect the interface between two materials with an in-line phase contrast imaging technique, i.e., the gap between two waves of the signal after the passage at the interface.¹⁹ The working energy of 17.6 keV is delivered by a single harmonic undulator and corresponds to an almost monochromatic beam ($\Delta\lambda/\lambda=5.10^{-2}$). Moreover, this beam flux is very high and therefore improves the contrast and decreases the acquisition time. In this case, a scan of 300 radiographs over 180 degrees took 9 s (Fig. 1, top). In both cases, the acquisition time value

is small enough so that changes within the material during scanning, such as the motion of gas cells, can be disregarded.

A piece of dough was placed in a Plexiglas[®] tube to avoid beam absorption, with an internal diameter of 9 mm and a height of 40 mm, at the constant temperature of the hutch, set at +20°C/-1°C. Images were acquired at a voxel size of 15 μm (BM05) and 5 μm (ID19) every 10 and 5 min, respectively, for 3 hours, a realistic time value regarding the baker's fermentation process; each image contained 1024 x 1024 x 900 voxels. Different voxel sizes required different acquisition times because of the use of different equipment (objectives, scintillators, etc.), finally resulting in different energies with different photon fluxes. These voxel sizes lead to an experimental error in size measurement of +/-15 μm and +/-5 μm for the two series of experiments, whereas acquisition times lead to an uncertainty of +/-5 min and +/- 2 min 30 s.

2.3 3D image processing

The whole procedure of image processing and data treatment is schematically represented in Fig. 1. After 3D image reconstruction, the two contrasting sets of information are combined using an adapted algorithm, phase contrast for interfaces and absorption contrast for the gas and the starch/gluten matrix, in order to quantify the density in each voxel of the sample.²⁰ Given the resolution and the image size, the technique considers a local sample region of 5³ mm³. On the 3D images (32 bits), a pre-treatment converts images to eight bits. A Region of Interest (ROI) set at a given height of the tube is defined, and using ImageJ[®] software (ImageJ, <http://rsbweb.nih.gov/ij/>), an automatic segmentation step, including filtering, is applied to obtain binary images. Porosity is determined on the basis of these 3D binary images by the ratio of bubble volume to sample volume. A Representative Elementary Volume (REV) is then delineated once a constant porosity is obtained. Two types of analyses are then performed (Fig. 1, bottom):

(1) A granulometry analysis in order to determine the size distributions of bubbles and cell walls in the dough with their mean value and standard deviation. The granulometry analysis consists in morphological openings of increasing size, like image sieving.²¹ Granulometry makes it possible to determine a characteristic size of any connected space by comparison to a structural element (SE) of a given shape, octahedral in this case, taken as a size reference. It is therefore well adapted in this case since gas bubbles may deform and not maintain a spherical shape. This method has been described in detail by Turbin-Orger,¹⁴ and only some basic principles are recalled here. A connected set of the image voxels is modified

by the opening if one of its dimensions is smaller than SE. In the case of a spherical object, its size is the bubble diameter; if the object has a non-spherical shape, its size is defined as the size of the largest SE that it can contain. In the following, we still refer to it as “size” rather than radius because bubble shape is not always spherical. Conversely, cell walls are not individual objects but a continuous phase instead. A distribution of the size of SE that better fits the phase boundaries is determined by granulometry. Accordingly, this size is referred to as “thickness”. Overall, granulometry is well suited when the objects have ill-defined shapes or occupy a continuous phase. Accordingly, bubble and wall distributions are expressed as a volume fraction and not as a number of objects.

(2) Labeling makes it possible to determine the connectivity of bubbles in the dough. It is based on the assignment of a label for each bubble in the sample volume. It is relevant when the objects have to be identified and precisely delimited. This is the case for tracking bubbles, knowing their coordinates in the sample and their volume, and determining the evolution of their size. Labeling is also useful for the global characterization of the sample image, by the connectivity index I_{co} :

$$I_{co}(t) = (\text{Volume of the largest bubble})/(\text{Total bubble volume}) \quad (1)$$

This index, defined by Martin,²² may be initially interpreted as an indicator of coalescence. Indeed, an I_{co} value close to 0 suggests that all bubbles have a size of the same order of magnitude, whereas a value close to 1 means that the largest bubble has the same volume as the total void fraction, indicating that all bubbles are connected.

2.4 Confocal Laser Scanning Microscopy (CSLM)

Three dyes were used for specific staining of water, proteins and lipids: Oregon Green 488 (OG488, Invitrogen, Carlsbad, NM, USA), Rhodamin B (RB, Merck, Darmstadt, Germany) and Bodipy (BP, Invitrogen, Carlsbad, NM, USA), respectively. Their maximum excitation and emission wavelength is significantly different, so that their spectra only slightly overlap: Oregon Green 488 (498, 526 nm), Rhodamin B (573, 591 nm) and Bodipy (665, 676 nm).

The procedure is as follows. A 1-mM solution of OG is prepared in distilled water and a 5-mM solution of BP is prepared in DMSO. Protein staining is performed on a piece of dough removed after mixing according to the procedure described in Section 2.1, before lixiviating in order to remove starch freeze-drying and grinding. One hundred mg of the resulting powder is mixed with 50 mL of 10^{-4} RH solution, by gentle stirring for 6 h before dialysis for 48 h, freeze-drying and grinding. A total of 12.5 mg of this powder and 32 μ L of

BP solution are added to 5 g flour, in the composition of # 1 (Table 1) before manual mixing in a mortar with 3.1 mL water containing 1% OG solution.

Resulting dough pieces are slightly squeezed between two glass blades and placed on the microscope (Nikon, Ti-E, A1) for continuous observation until 180 min proofing using x 1.4 and eight zooms with an objective of x 20, which leads to the highest resolution, corresponding to a pixel size of $1 \mu\text{m}^2$.

3. Results and discussion

3.1 Experiments at a voxel size of $15 \mu\text{m}$: development of the cellular structure

First, images are extracted in order to observe the different sequences of bubble growth and cellular structure development during fermentation of the various wheat flour doughs. For easier comparison, only 2D sections, obtained for dough # 6, (“baguette”) are represented (Fig. 2). They clearly present an increase over time of the dark areas (bubbles), whereas light gray ones featuring the starch/gluten matrix of the dough decrease over time. This increase is due to the production of gas, mainly CO_2 , by yeast. At the beginning, the microstructure is quite homogeneous, with a large number of small bubbles. It subsequently becomes more and more heterogeneous, with large and deformed bubbles connected to each other at the end of fermentation ($t=166$ min in Fig. 2). These general trends were observed for all dough compositions.

3.1.1 Quantitative analysis of bubble growth and cellular structure development.

These observations may be ascertained by the evolution of the bubble size and cell wall thickness distributions obtained after granulometry analysis of the 3D images since a REV is determined in every case (Figs. 2a and b). Twenty-seven bubble size distributions are represented together, first by their volume fraction (inserted into Fig. 2a). They show a decrease of the peak representing bubbles of smaller size and its continuous translation when fermentation time increases to 166 min, from lower values ($< 100 \mu\text{m}$) to higher ones ($> 400 \mu\text{m}$), with a $15 \mu\text{m}$ experimental uncertainty due to voxel size. The wavy shape of the volume distribution for larger sizes is explained by the size of the ROI from which a bubble can partly escape at a given fermentation time, whereas another one of larger size may appear later. To avoid this graphical drawback, we also represent the cumulative volume distributions, which clearly display a continuous spreading over fermentation time. This spreading is marked by a

continuous increase of the average bubble size from 160 μm to 980 μm and standard deviations from 150 to 630 μm , as well as a decrease of the maximum slope of the sigmoid curves. This decrease reflects an increase in the heterogeneity of cellular structure since at higher fermentation times, small bubbles can still be contiguous to larger ones (up to 1.6 mm). In the following, the maximum slope of this curve is taken as an index of homogeneity of the cellular structure. Secondly, this graph also shows a continuous decrease of the volume fraction, from 0.16 to 0, associated with smaller bubbles (30 μm). These results overall reflect the continuous but non-uniform growth of gas bubbles in the matrix.

The wall thickness distributions follow a normal distribution but do not evolve in the same monotonous way (Fig. 2b). They continuously spread with fermentation time, which confirms the increase of heterogeneity of the cellular structure. There is a pronounced increase in the fraction of thinner walls ($\approx 80 \mu\text{m}$) with fermentation time, which appears concomitant to the growth of bubbles: the larger the bubbles are, the more closely packed they become, and the thinner the wall separating them will be. Conversely, the initial peak, close to 300 μm , moves to a minimum value of around 250 μm after 1 h fermentation. The thickness then increases once again, up to 300 μm , whereas the fraction of larger walls ($\geq 400 \mu\text{m}$) seems to follow the same trend as the peak. This last result suggests that, for longer fermentation times, the evolution of cellular structure does not obey a simple mechanism of bubble growth. The trends observed here have been checked for the different dough compositions, using average quantities to characterize distributions, in order to extend the interpretations proposed.

Porosity kinetics give an overview of bubble growth in the dough matrix (Fig. 3a). All curves display similar features, *i.e.*, a sigmoid shape with a continuous increase to an asymptotic value close to 0.7. All these kinetics present an inflexion point at a time value t_p ranging from 22 min (#1) to 65 min (#3), for approximately the same porosity value, $P \approx 0.27$. The slower kinetics are obtained for dough with a small amount of yeast (#5) or a high level of sugar (#3). Both conditions imply a reduction in gas production since, in the second case, the high content of sugar probably inhibits yeast activity, due to osmotic stress.^{4,14,16}

The index of connectivity I_{co} , defined by the ratio of the volume occupied by the largest cavity to the total void volume, also displays a sigmoid shape, with, nonetheless, a sharper increase at a time value t_c , depending on dough composition (Fig. 3b). Clearly, this transition would be less sharp if the voxel size was smaller, but it would lead to the same value of t_c in the end. This evolution suggests that bubbles largely interact when $t > t_c$, before they become massively connected ($I_{co} \approx 1$) and can coalesce, thus suggesting that the gas

phase could percolate at this resolution. In addition to doughs #3 and #5 ($t_c = 80$ min), as in the case of porosity, a large t_c value is also reached for dough #4, characterized by a higher value liquid fraction Φ_v (Table 1). Conversely, other doughs (#1, #2, #6) with low sugar and liquid fractions have a short connectivity time ($30 < t_c \leq 35$ min).

A mean value is determined on the basis of the wall thickness distribution, designated *MCWT* for all compositions. Dough #4 with its large liquid fraction exhibits the largest mean wall thickness values ($250 \leq MCWT \leq 360$ μm). For all of the doughs, the evolution of *MCWT* during fermentation is not monotonous and exhibits a minimum at a time value t_{wt} in the interval [34, 80 min] (Fig. 3c). This trend confirms the one observed from the distributions presented for dough #6 (Fig. 2b). For $t \leq t_{wt}$, the decrease of wall thickness is consistent with simple bubble growth. Conversely, for $t \geq t_{wt}$, the increase suggests the existence of thicker walls, but it could also reflect the disappearance of thinner walls either because of bubble coalescence or because their thickness becomes lower than the voxel size.

Using the bubble width distribution curves, we can see that the homogeneity index, defined as the maximum slope of these curves, continuously decreases after a short but significant increase during the earlier fermentation times (30 min for dough #3) (Fig. 3d). Clearly, this brief increase in homogeneity may be attributed to the disappearance of smaller size bubbles, already observed in Fig. 2a, which merge into larger ones through the effect of disproportionation, or Ostwald ripening.

The experimental error due to voxel size leads to a standard deviation of 15 μm for mean cell wall thickness, and a low standard deviation for porosity, connectivity and homogeneity indices (< 5%).

Finally, when summarizing the characteristic times derived from the evolutions of porosity, connectivity and cell wall thickness, as reported in Table 1, it was found that the three sets of time values t_P , t_c and t_{wt} , respectively, are correlated and, within experimental error, $t_c = t_{wt}$ (Fig. 3e). Given the sensitivity of I_{co} to the voxel size, this result is quite significant. It shows that the mechanisms of cellular structure development are concomitant. In particular, it suggests that before bubbles are connected, when $t < t_c$, they can grow “freely” due to gas production by yeast, without interacting with each other, and their growth is limited by the rheological properties of the starch/gluten matrix.

3.1.2 The first regime: free bubble growth. The hypothesis of free bubble growth when $t < t_c$, needs to be established. For this purpose, bubbles were individually tracked using a labeling technique. The evolution of their radius R is represented, for various initial radii R_0 ,

for dough # 5, which was taken as an example (Fig. 4; see insert). These kinetics are well fitted by an exponential function:

$$R(t) = R_0 e^{kt} \quad (2)$$

For a given dough, by derivation of $R(t)$, k defines the strain rate of the starch/gluten matrix due to the growth of a bubble of radius R :

$$k = \dot{\varepsilon} = \frac{1}{R} \frac{dR}{dt} \quad (3)$$

since bi-extension is the relevant mode of deformation of the matrix. The values of $\dot{\varepsilon}$ for all of the doughs vary between 10^{-4} and $4 \cdot 10^{-4} \text{ s}^{-1}$ (Fig. 4). They slightly decrease with R_0 : the smaller the bubbles are, the faster they grow and deform the surrounding viscous matrix.

In the case of free bubble growth in a viscous medium of viscosity η , according to Arefmanesh and Advani,²³ if the surface tension is ignored:

$$\frac{1}{R} \frac{dR}{dt} = \frac{P_v}{4\eta} \quad (4)$$

where P_v is the internal gas pressure of the bubble due to CO_2 production by yeast activity, diffusion in the viscous matrix, followed by vaporization into the bubble. Given the rheological properties of dough ($\eta = K \cdot \dot{\varepsilon}^{(n-1)}$), η can be computed using the data reported in Table 1 for typical values of $\dot{\varepsilon}$ plotted in Fig. 4. Taking $P_v = 1 \text{ kPa}$ as a typical value of bubble internal pressure,²⁴ computed values of k vary in the interval $[5 \cdot 10^{-5}, 5 \cdot 10^{-4} \text{ s}^{-1}]$. This interval covers the interval of values determined experimentally. A more accurate computation would involve the variations of CO_2 concentration and diffusion due to the sugar content.

This result confirms that bubble-free growth is the main mechanism of the first fermentation regime, and it provides a time value ($t = t_c$), depending on dough matrix viscosity and internal gas pressure, after which other mechanisms may prevail. Indeed, beyond this time value, bubbles can no longer be tracked, either because they escape the ROI, or because they deform and became connected to the other bubbles in the vicinity. To elucidate these mechanisms, X-ray tomography experiments were carried out at higher resolutions.

3.2 Experiments at voxel size = 5 μm : focus on the end of fermentation

In this second series of experiments (voxel size = 5 μm), only 2% of yeast is added to the wheat flour instead of the 3% in the preceding series, in order to slow down the bubble

growth and to better focus on bubble interactions at longer fermentation times and, therefore, higher porosities. Another recipe (#7) was added to favor the study of the possible effects of lipids.

3.2.1 The second regime: bubble connection. Under these conditions, the selection of a large enough porosity value (≈ 0.64) leads to high values of the connectivity index ($I_{co} \geq 0.8$; see Table 1), which ensures that bubbles are largely connected for all of the doughs, for values of fermentation time in the interval [120, 190 min]. The fact that this porosity value is the same as the maximum random packing fraction of monodisperse spheres here is a coincidence.

For these time values and the same porosity value, cell wall thickness and bubble size distributions are therefore represented together (Fig. 5a, b). They clearly show that even for the same value of porosity, different compositions lead to different cellular structures. This is also illustrated by the 3D images inserted into Fig. 5a, where large deformed bubbles, or gas cavities, interpenetrating each other, may be observed. All distributions of wall thickness follow a normal distribution and display a peak close to $230 \pm 30 \mu\text{m}$ (Fig. 5b). Their mean values (*MCWT*), vary from 170 to 260 μm . The maximum size of gas cells ranges from 1.3 to 2 mm, with mean values (*MCS*) in the interval [400, 830 μm]. We chose to represent the bubble distribution by *MCS* rather than by the homogeneity index (Fig. 3d) because, far from the initiation of the first regime, disproportionation is unlikely and *MCS* is more meaningful here for the purpose of comparison. Indeed, both cellular structural features, *MCWT* and *MCS*, are correlated, as illustrated by the graph inserted in Fig. 5b, where this trend is emphasized by taking the values derived from the first series into account as well. This result shows, for the same porosity, first, that dough cellular structures may range from coarser, with large bubbles and walls, to thinner, with smaller bubbles and narrower walls and, second, that the cellular structure obtained is independent of the yeast quantity in the interval [1.5, 3% flour] and, consequently, of the porosity kinetics. Comparison with data from Table 1 also suggests that for same yeast content, coarser cellular structures ($MCS \geq 800 \mu\text{m}$) are instead obtained for larger values of the liquid fraction ($\Phi_{vl} \geq 0.6$).

In addition to these average indications, 3D images (Fig. 5a) show the presence of large gas cell cavities, or gas cells (in order to differentiate them from “bubbles”), which reflects the heterogeneity of the cellular structure. The complex shape of these cavities suggests that they might be formed by several bubbles separated by thin walls (Fig. 6a), which

sometime seem to contain holes (Fig. 6b). Since the volume fraction of the thinnest walls ($\leq 5\mu\text{m}$) is not null ($\geq 10^{-4}$), these holes may be an image artifact rather than evidence of coalescence initiation. Consequently, connected bubbles are probably separated by walls that have a thickness that is less than the voxel size ($5\mu\text{m}$) and that could not be detected for this XRT resolution. This is also revealed by the 2D scans, which enhance the fineness of the walls separating the bubbles (Fig. 6c). Their fineness is underlined by the black/white fringe (Fig. 6 d, e). It is tempting to directly attribute the black/white fringe at the gas/matrix interface to a third phase, liquid, resulting from demixing or syneresis in the dough matrix, and which would form liquid films after continuous stretching by the growth of gas cells, but we believe that on these images, it is instead due the local absorption contrast. However, given the size of starch granules ($> 5\mu\text{m}$), these walls cannot contain starch granules. Moreover, due the low gluten content ($\approx 7\%$ of the total), the existence of a continuous gluten phase is unlikely. These results confirm the hypothesis of the presence of liquid films separating bubbles, observed by scanning electron microscopy.²⁵ In fact, the coalescence of bubbles would lead to gas percolation and dough collapse during the final step of fermentation, whereas the presence of liquid films would prevent this phenomenon. These liquid films would be composed of hemicelluloses and surface-active biopolymers, polar lipids or low molecular weight proteins.^{26,27} They would burst during baking at a temperature in the same range as gluten cross-links and the starch granules would swell, leading to the dough/crumb transition and open cellular structure of the crumb.²⁸

Thanks to component staining, CSLM observations helped to establish this hypothesis. In the micrograph of dough #6 after 2 h fermentation (Fig. 7a), the hydrophilic parts appear in green (w), proteins in red (p) and lipids in blue (l). Other colors result from the superimposition of these elementary colors. They reveal the area that contains about the same amount of several components: yellowish parts reflect the coexistence of protein with hydrophilic parts (starch), featuring the starch/gluten matrix. Black parts are the gas bubbles. Lipids, endogenous or added, are predominantly located at the interface between the matrix and bubbles and are clearly distinct from the hydrophilic parts. A lipid film containing a droplet of water separates gas bubbles. It is too thin ($< 5\mu\text{m}$) to contain any starch granules. A focus on such a film (Fig. 6b) highlights the presence of an aqueous phase (a) in addition to lipids (L) and, to a lesser extent, proteins (p). The absence of yellow, in contrast with the matrix, shows that proteins do not mix with the hydrophilic phase, so these proteins would not be gluten but, instead, low-molecular-weight proteins competing with lipids to migrate at the

bubble interface.²⁶ These films are therefore not only aqueous but consist of an emulsion of hydrophilic compounds and lipids.

These observations are consistent with the hypothesis of the existence of liquid films in the cellular structure of the dough. Therefore, to summarize, a structural scheme of fermented wheat flour dough can be proposed. It assumes that when dough has a high level of porosity, bubbles are highly connected to each other, only separated from their neighbors by thin liquid films. Consequently, at the end of fermentation, dough may be seen as a three-phase medium: gas (entrapped air + gas produced by yeast), liquid phase (oil/water emulsion including low molecular weight proteins) and a viscoelastic matrix (starch + gluten) (Fig. 8). Due to the low thickness of the walls, starch granules instead gather at the corners of the structure, *i.e.*, the Plateau border by analogy with liquid foams. Consequently, the edges of the cubic cell are constituted of gluten filaments, whereas liquid films form the walls that separate gas cells.

3.2.2. From microstructure to macroscopic behavior: the contribution of different phases to dough stability. Based on the preceding description, and analogous with the approach described for biphasic media such as emulsions or liquid foams,²⁹ we define an apparent capillary number in order to integrate the influence of the various levels of organization of dough represented in Fig. 8:

$$Ca^* = (\tau_m \cdot MCWT^2)/(\gamma \cdot MCS) \quad (5)$$

τ_m is the elongational stress exerted by the gas cell on the starch/gluten matrix, and γ is the surface tension of the dough liquid phase. The elongational behavior of the dough matrix determined by uniaxial compression under lubricated conditions¹⁸ is not Newtonian, and the variations of the elongational viscosity η , with strain rate $\dot{\epsilon}$, can be fitted by a power law:¹⁷

$$\eta = K \cdot (\dot{\epsilon})^{n-1} \quad \text{for a constant strain } \epsilon_b \quad (6)$$

The values of the consistency index K and the flow behavior index n are reported in Table 1. They were determined by Turbin-Orger³⁰ for the same dough compositions at a strain value of $\epsilon_b = 1$. τ_m can therefore be computed for an average strain rate value of $\dot{\epsilon} = 2 \cdot 10^{-4} \text{ s}^{-1}$, in accordance with Fig. 4, leading to values in the interval [50, 600 Pa].

The surface tension γ was determined for the liquid phase extracted from the various doughs by ultracentrifugation, referred to as dough liquor. This dough liquor has a density of

1.1 g/mL,²⁷ close to that of dough (1.2 g/mL, according to Bellido),¹² making its detection by XRT challenging. It is considered to be a good model of the dough liquid phase,²⁶ *i.e.*, of the liquid films separating gas cells. Its value, measured by the pending drop method, mainly varies from 35 to 41 mN/m, according to the content of dough liquor in arabinogalactan-protein.²⁷ These macromolecules, a complex of polysaccharides and proteins, are probably present in the liquid films observed at the gas cell interface (Fig. 7).

The values of $MCWT$, the mean cell wall thickness, taken here as the value of gluten filament thickness, and MCS , chosen as the average radius of gas cells, are those reported in Table 1, *i.e.*, for $P = 0.64$. Their variations lead to a change in the ratio ($MCWT^2/MCS$) by a factor of 2.

By implementing these values in eq. (5), it is possible to compute Ca^* , which leads to values in the interval [0.1, 1]. Clearly, the elongational properties of the dough matrix contribute the most to these variations in comparison to cellular features, whereas dough liquor properties only slightly influence Ca^* , at least in the range of the composition tested. The poor influence of the liquid phase should be qualified since it is expected that the coalescence will be more effectively controlled by the high frequency elasticity, as shown for air bubbles in water and soap.³¹ Perhaps this property would be more relevant than surface tension, although in the case of dough liquor, it was found to be relatively constant, close to 0.5 mN/m.²⁶ Conversely, a variation by a factor of 2 of the ratio ($MCWT^2/MCS$) may later reflect significant changes in the final crumb appearance since cellular structural features are not significantly modified by baking.

It is therefore interesting to use Ca^* in order to explain the macroscopic behavior of wheat flour dough, which expands (the porosity increases) and slowly spreads during fermentation. These phenomena, expansion and spreading, have already been assessed by the follow-up and 2D image analysis of dough volume and shape, respectively. Extensive spreading or loss of stability is clearly undesirable and is often associated with internal collapse due to gas cell coalescence.^{17,25,26} It has been quantified by the kinetics of the shape factor of a free-standing round piece of dough during fermentation, and fitted by an exponential decay function:³²

$$H / L_{max}(t) = a' \cdot \exp(-t/b') + c' \quad (7)$$

H and L_{max} are the height and maximum width of the piece of dough, respectively. The lower the characteristic time b' is, the more rapidly the dough spreads and the less stable it is. The values of Ca^* computed for all of the doughs are found to increase with b' , the characteristic time of stability (Fig. 9): the more viscous the starch-gluten matrix is, the lower the surface tension of the dough liquor will be, the smaller the bubble size will be and the more stable the piece of dough will be. Clearly, the correlation could be improved if the precise values of the cellular structural features of other doughs could also be determined by XRT, instead of taking average values for MCS and $MCWT$.

Conversely, once b' is determined by simple macroscopic measurements of the dough development, a value of Ca^* can be deduced from the correlation represented in Fig. 9. Subsequently, once the extensional properties of the dough are measured and the wheat arabino-galactan content is known, hence the value of γ , the ratio ($MCWT^2/MCS$) can be derived using eq. (5), and useful information about the dough cellular structure at the end of fermentation can be inferred.

4. Conclusion

By using a synchrotron source for short acquisition times, X-ray tomography, supplemented with 3D-image analysis, has shown itself to be a powerful technique to reveal the various mechanisms involved in the development of a gas cellular structure in a highly viscous opaque medium, wheat flour dough in this case. By implementing it for two different resolutions and various dough compositions during fermentation, we determined the cellular features after image analysis, *i.e.*, porosity, connectivity, gas cell size and cell wall thickness distributions, and their evolution. The comparison of these kinetics shows that bubbles first grow freely before they connect to each other and possibly coalesce. A first regime could be identified by tracking individual gas bubbles, which also shows that their strain rate is governed by the ratio of gas pressure to viscosity, in agreement with simple models of free bubble growth. Higher resolution analysis of the second regime, *i.e.*, at larger porosity values, shows that very distinct cellular structures are obtained for different compositions. 3D images suggest that bubble coalescence is limited by liquid films that separate gas bubbles. Together with these observations, the use of confocal scanning laser microscopy (2D) to localize dough components suggests that the fermented dough is a three-phase medium: gas cells and liquid film walls are embedded in the composite matrix of starch granules, located in the cell corner, with gluten filaments constituting the beams of the gas cells. By considering a scheme of a

dough structure element, these levels of organization were integrated, and an apparent capillary number Ca^* could be defined. It is the ratio of dough matrix elongational forces to the liquid surface tension forces. By computing Ca^* values, it is possible to assess the contribution of the different phases to dough macroscopic behavior, and to infer the stability of the dough at the macroscopic scale. Various prospects can be imagined using this technique for *in situ* experiments, such as focusing on the possible contrast between liquid and matrix phases, or determining the possible cellular orientation during material shaping operations.

Acknowledgements

The research that led to these results received funding from the European Community's Seventh Framework Programme (FP7/ 2007-2013) under the grant agreement n°FP7-222 654, Dream project: Design and development of REAListic food Models with well characterized micro- and macro-structure and composition. The authors are also grateful to the ESRF staff (beamlines BM05 and ID19) and especially to Peter Cloetens and Paul Tafforeau for their valuable advice.

References

- 1 A. Donald, *Nature Mat.*, 2004, **3**, 579-581.
- 2 M.A.V. Axelos, *DREAM. European Community's Seventh Framework Programme (FP7/ 2007-2013, grant agreement n°FP7-222 654)*, 2014, <http://dream.aaeuropae.org/>
- 3 L. J. Gibson and M. F. Ashby, *Cellular Solids*, Cambridge University Press, UK, 1997, 510p.
- 4 M.C. Zghal and M.G. Scanlon, *Food Res. Int.*, 2001, **34**, 841-864.
- 5 M. A. P. Mohammed, M.N. Tarleton, M. N. Charalambides and J.G. Williams, *J. Rheol.*, 2013, **57**, 249-272.
- 6 I.C. Bache and A.M. Donald, *J. Cereal Sci.*, 1998, **28**, 127-133 .
- 7 N. Ishida, H. Takano, S. Naito, S. Isobe, K. Uemura, T. Haishi, T. Kose, M. Koizumi and H. Kano, *Mag. Reson. Imaging*, 2001, **19**, 867-874.
- 8 H.M. Elmehdi, J.H. Page, and M.G. Scanlon, *Trans. Ichem E.*, 2003, **81**, 217-223.
- 9 E. Maire, A. Fazekas, L. Salvo, R. Dendievel, S. Youssef, P. Cloetens and J.M. Letang, *Comp. Sci. Tech.*, 2003, **63**, 2431-2443.
- 10 P.M. Falcone, A. Baiano, F. Zanini, L. Mancini, G. Tromba, F. Montanari and M. Del Nobile, *J. Food Sci.*, 2004, **69**, 38-43.
- 11 B.R. Pinzer, A. Medebach, H.J. Limbach, C. Dubois, M. Stamponi and M. Schneebeli, *Soft Matter*, 2012, **8**, 4584-4594.
- 12 G.G. Bellido, , M.G. Scanlon, J.H. Page, and B. Hallgrimsson, *Food Res. Int.*, 2006, **39**, 1058-1066.
- 13 P. Babin, G. Della Valle, H. Chiron, P. Cloetens, J. Hozowska, P. Pernot, A.L. Reguerre, L. Salvo, L. and R. Dendievel, *J. Cereal Sci.*, 2006, **43**, 393-397.
- 14 A. Turbin-Orger, E. Boller, L. Chaunier, H. Chiron, G. Della Valle, A-L. Réguerre, *J. Cereal Sci.*, 2012, **56**, 676-683.
- 15 W. Li, B.J. Dobraszczyk and P.J. Wilde, *J. Cereal Sci.*, 2004, **39**, 403-411.
- 16 A. Romano, G. Toraldo, S. Cavella and P. Masi. *J. Food Eng.*, 2007, **83**, 142-148.
- 17 T. van Vliet, A.M. Janssen, A.H. Bloksma and P. Walstra, *J. Texture Studies*, 1992, **23**, 439-460.
- 18 S.H. Chatraei, C.W. Macosko and H.H. Winter, *J. Rheol.*, 1981, **25**, 433-443.
- 19 J. Baruchel, P. Bleuët, A. Bravin, P. Coan, E. Lima, A. Madsen, W. Ludwig, P. Pernot, P. and J. Susini, *C. R. Phys.*, 2008, **9**, 624-641.
- 20 E. Boller, P. Tafforeau, W. Ludwig, L. Helfen, T. Weitkamp, L. Salvo, P. Cloetens and J. Baruchel, *Conference Matériaux*, Nantes, 2010.

- 21 P. Soille, *Morphological image analysis*, Springer, Berlin, 2003, 391p.
- 22 C.F. Martin, C. Josserond, L. Salvo, J.J. Blandin, P. Cloetens and E. Boller. *Scripta Materialia*, 2000, **42**, 375–381.
- 23 A. Arefmanesh and S.G. Advani, *Rheol. Acta*, 1991, **30**, 274-283.
- 24 D. Grenier, D. Le Ray and T. Lucas, *J. Cereal Sci.*, 2010, **52**, 373-377.
- 25 Z. Gan, P.R. Ellis and J.D. Schofield, *J. Cereal Sci.*, 1995, **21**, 215-230.
- 26 L.J. Salt, P.J. Wilde, D. Georget, N. Wellner, P.K. Skeggs and E.N.C. Mills, *J. Cereal Sci.*, 2006, **43**, 284-292.
- 27 A. Turbin-Orger, G. Della Valle, J-L., Doublier, A-L. Fameau, S. Marze and L. Saulnier, *Food Hydrocolloids*, 2015, **43**, 114-124.
- 28 S. Wang, P. Austin and S. Bell, *J. Cereal Sci.*, 2011, **54**, 203-210.
- 29 R.G.M. van der Sman and A.J. van der Goot. *Soft Matter*, 2009, **5**, 501-510.
- 30 A. Turbin-Orger, A. Shehzad, L. Chaunier, H. Chiron and G. Della Valle, to *J. Food Eng.*, submitted.
- 31 D. Georgieva, A. Cagna and D. Langevin. Link between surface elasticity and foam stability. *Soft Matter*, 2009, **5**, 2063-2071.
- 32 A. Shehzad, H. Chiron, G. Della Valle, K. Kansou, A. Ndiaye and A. L. Réguerre, *Food Res. Int.*, **43**, 1999-2005.

Figures list

Figure 1: Schematic graph of the image analysis procedure. Final analysis techniques, granulometry and labeling, as detailed in the text, are applied after determining a representative elementary volume (REV).

Figure 2: Evolution of volume fractions (a) cumulative for gas cell size (with non-cumulative distribution inserted) and (b) for cell wall thickness distributions of dough # 6 (62% added water) with corresponding 2D images taken at the sample median plane, for three fermentation times: 0, 60 and 166 min.

Figure 3: Kinetics of the main cellular features during fermentation of doughs #1 (●), 2 (▲), 3 (■), 4 (○), 5(-), 6 (□): porosity (a); connectivity index ($I_{co}=0$, all bubbles are separated; $I_{co}=1$, all bubbles are connected) (b); mean cell wall thickness (*MCWT*) (c); and homogeneity index (maximum slope of bubble size distributions) (d); and variations of characteristic times derived from these kinetics: inflexion point of porosity curves t_p (●) and minimum of *MCWT* (○) as a function of the inflexion point of I_{co} (e). The standard deviation is 15 μm for mean cell wall thickness, and lower than 5% for porosity, connectivity and homogeneity indices.

Figure 4: Variations, with initial bubble radius, of strain rate computed from kinetics of bubble growth (example inserted for dough # 5, each dot representing one bubble, followed during fermentation) according to eq. (3) for doughs #1 (●), 2 (▲), 3 (■), 4 (○), 5(-), 6 (□).

Figure 5: (a) Volume distributions of cell wall thickness (including corresponding 3D images for dough #1 and #7; cube edge: 4 mm; voxel size: 5 μm) and (b) cumulative volume distribution of gas cell size for the second series of experiments, including the graph of variations of *MCS* vs. *MCWT* for dough containing 3% yeast (●, first series) and 2% yeast (○, second series) ($r^2=0.81$), all taken for the same porosity values = 0.64 for dough ●: #1; ○: #4; ▲: # 6; and □: #7.

Figure 6: Typical binary 3D images of fermented dough with a porosity $P = 0.64$ (#1 here after 125 min fermentation, matrix in white, voxel size = 5 μm) (a) cube edge: 2.5 mm, with (b) focus on bubble interface (upper edge: 1.5 mm); and (c, d, e) 2 D scans (white bar =

50 μm , matrix in light gray, bubbles in dark gray) of doughs #1, 2 and 3, respectively, focusing on walls separating bubbles.

Figure 7: CSLM views (a) of dough #1 matrix with two gas bubbles, and (b) focus on liquid films at dough bubble interface after 120 min fermentation; green: hydrophilic parts (w); red: proteins (p); and blue: lipids (l or L); “a” indicates aqueous (hydrophilic) phase, “b” gas bubbles, and “m” dough matrix.

Figure 8: Proposed scheme of a structure element representing gas cells embedded in the composite matrix of starch granules/gluten filaments, with liquid film walls.

Figure 9: Variations of apparent capillary number Ca^* vs. characteristic time of macroscopic stability, determined by Turbin-Orger,³⁰ for dough observed by XRT (●) and other compositions (O) for which Ca^* was computed from average values of MCS and $MCWT$. Fitting is performed for the first set ($r^2 = 0.78$).

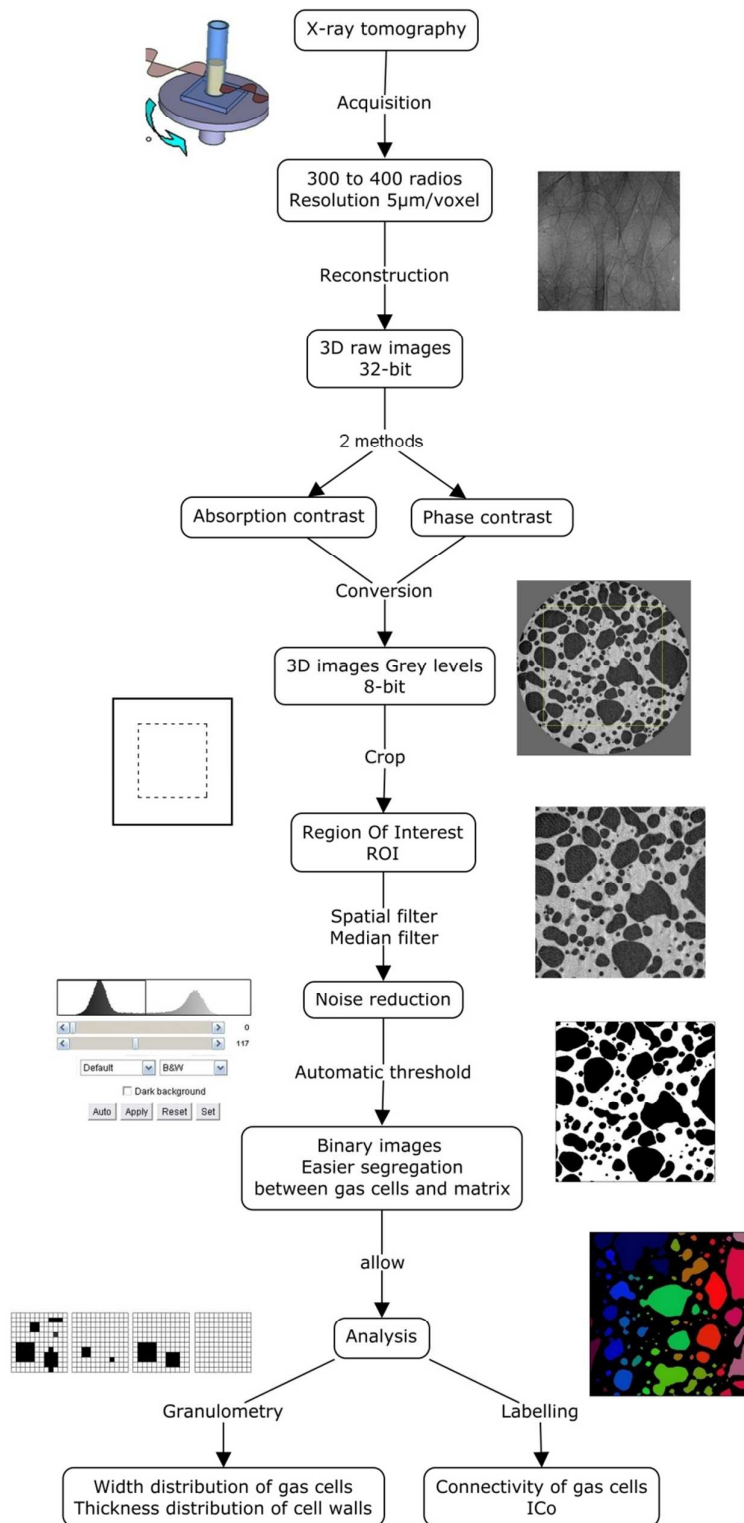


Figure 1

*Bubble growth in viscoelastic dough**Turbin-Orger et al.*

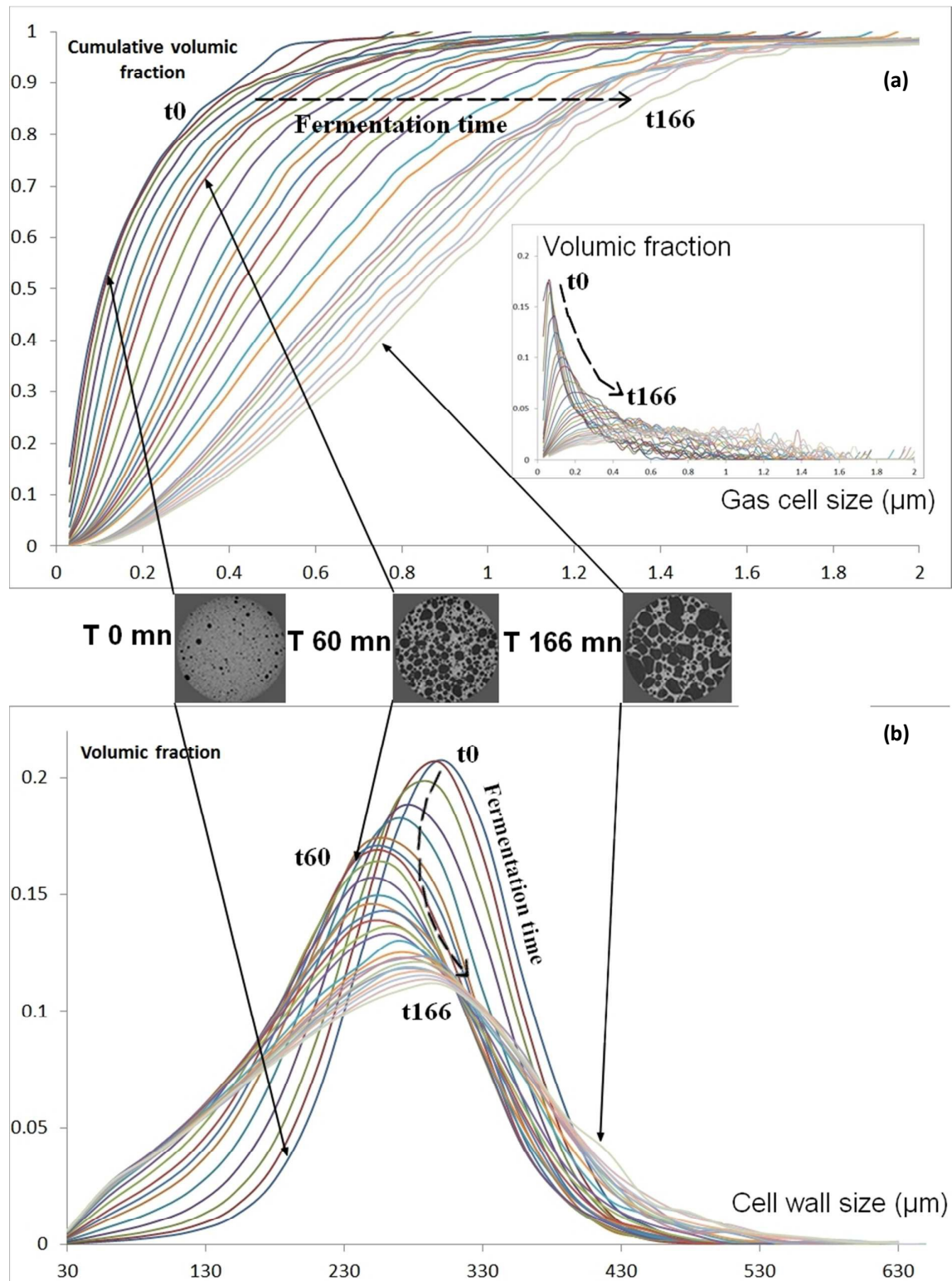


Figure 2

Bubble growth in viscoelastic dough

Turbin-Orger et al.

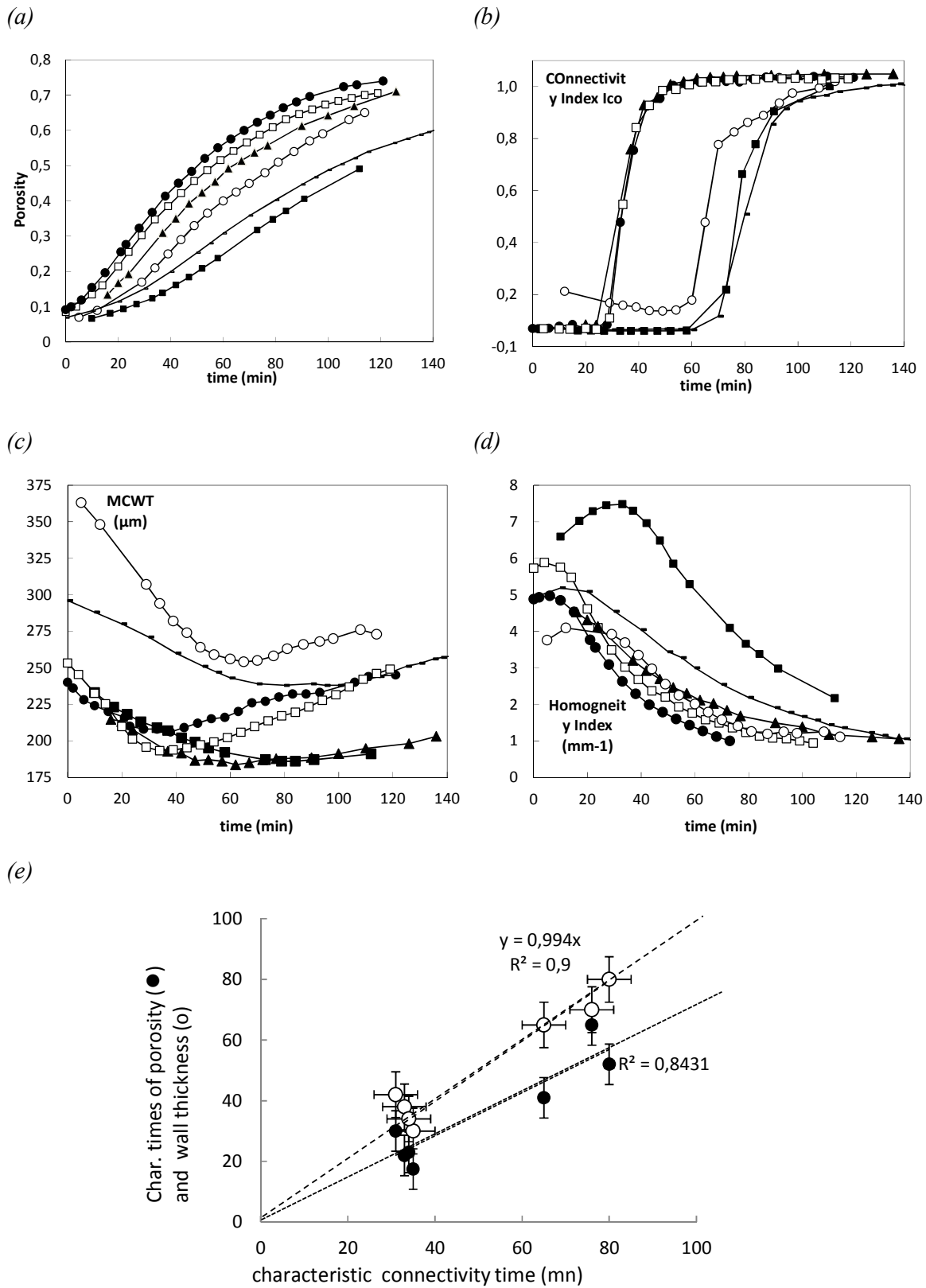


Figure 3

Bubble growth in viscoelastic dough

Turbin-Orger et al.

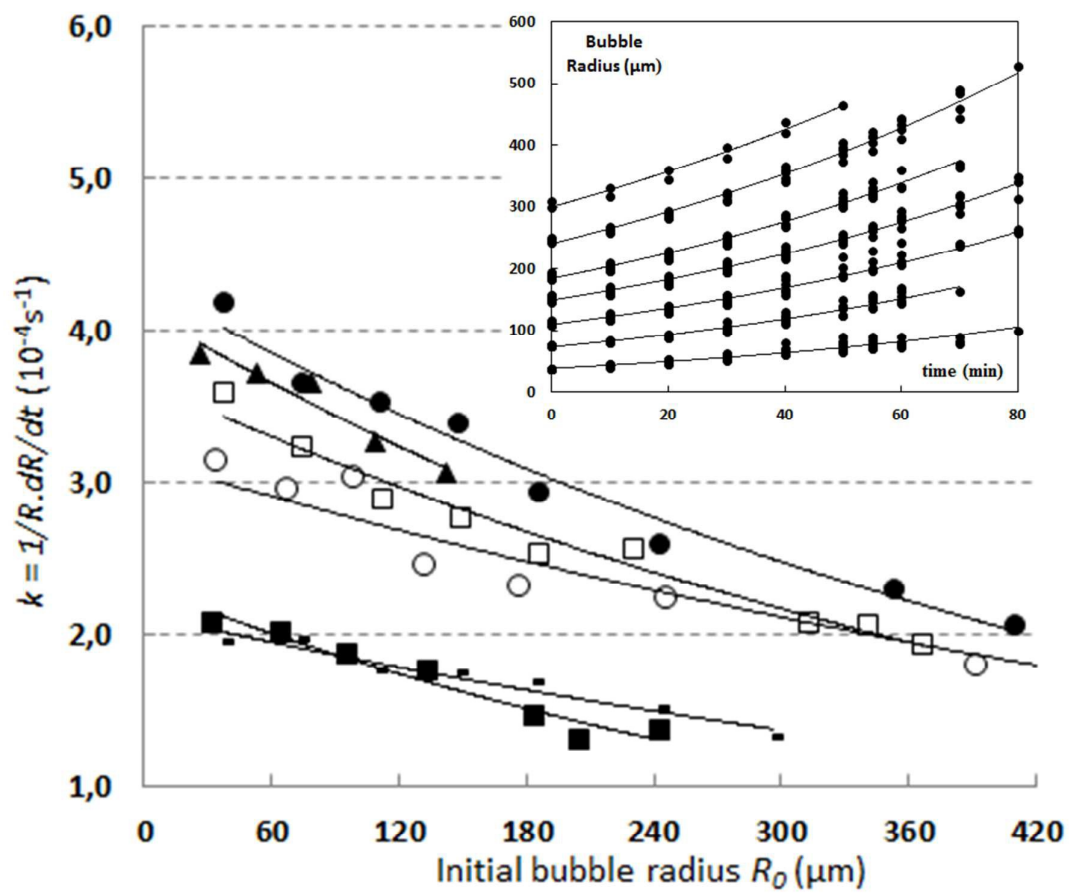


Figure 4 Bubble growth in viscoelastic dough Turbin-Orger et al.

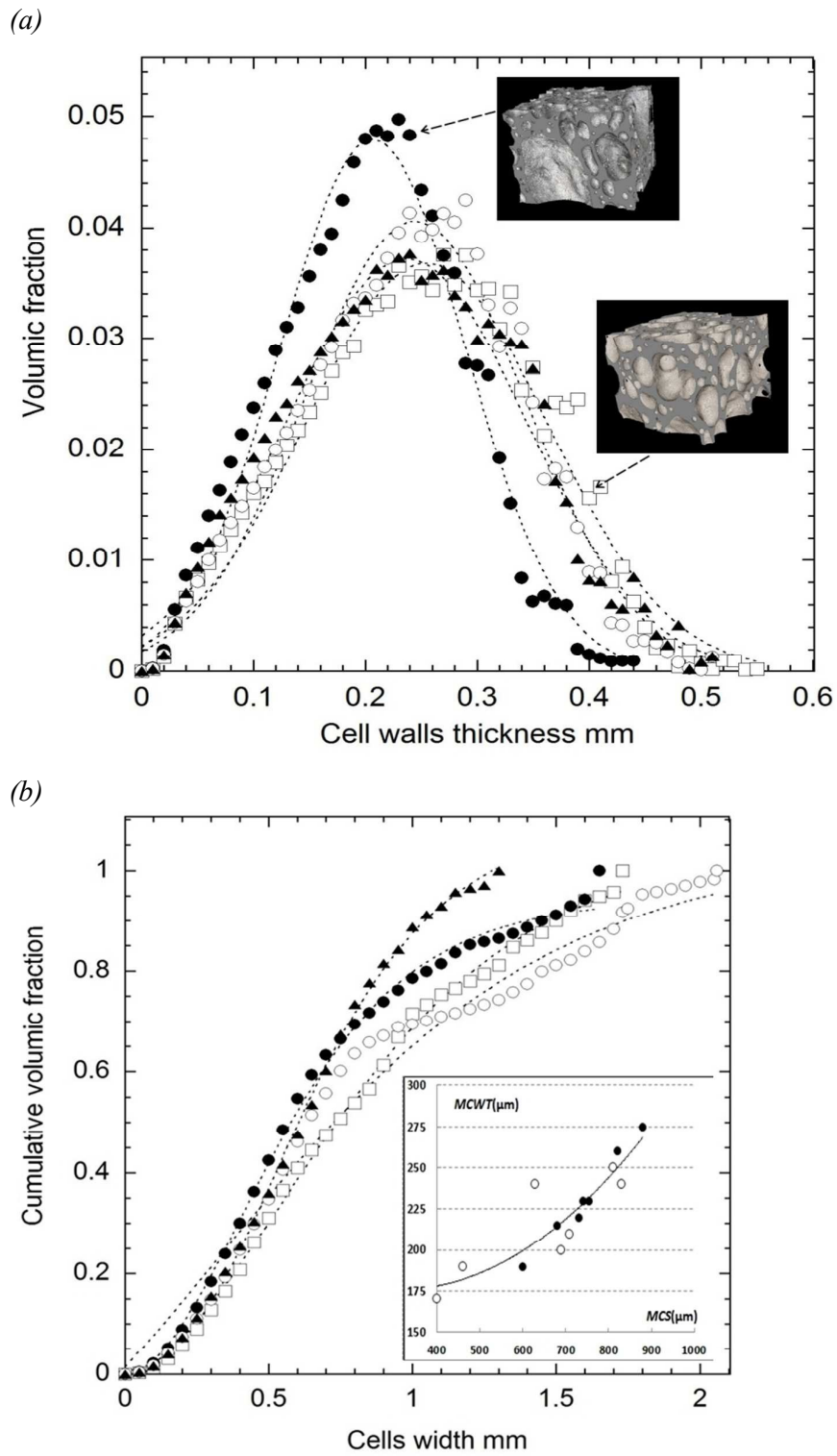


Figure 5

Bubble growth in viscoelastic dough

Turbin-Orger et al.

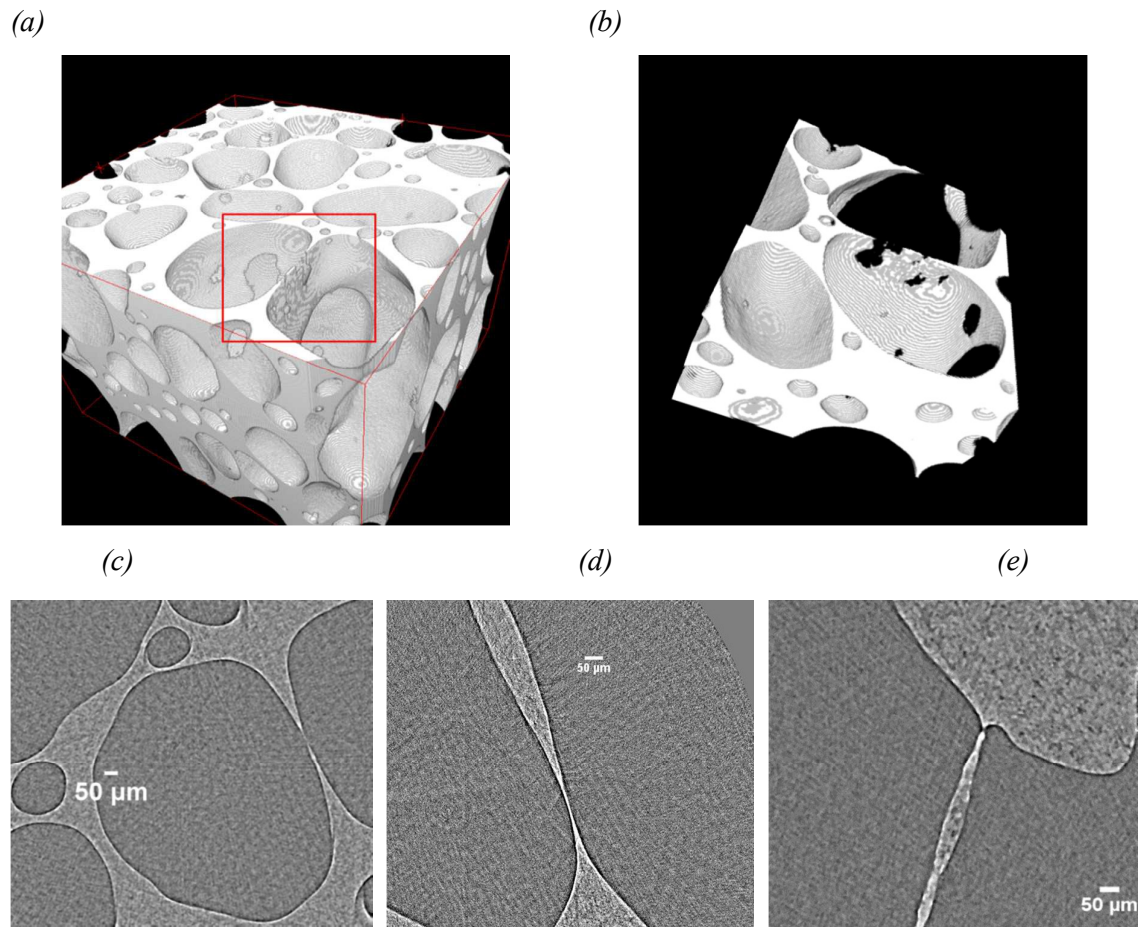
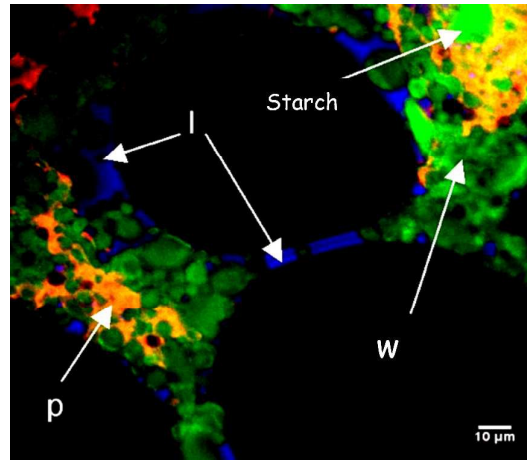


Figure 6 Bubble growth in viscoelastic dough Turbin-Orger et al.

(a)



(b)

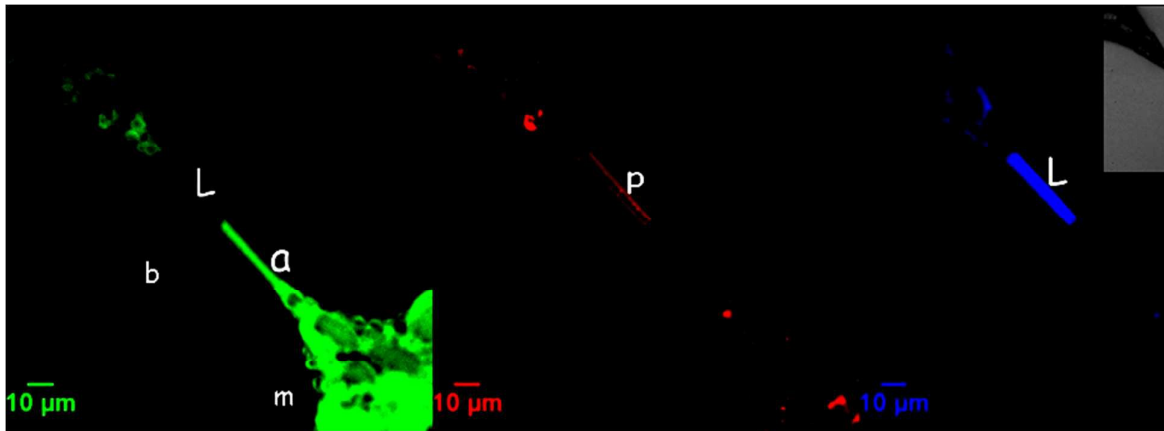


Figure 7

*Bubble growth in viscoelastic dough**Turbin-Orger et al.*

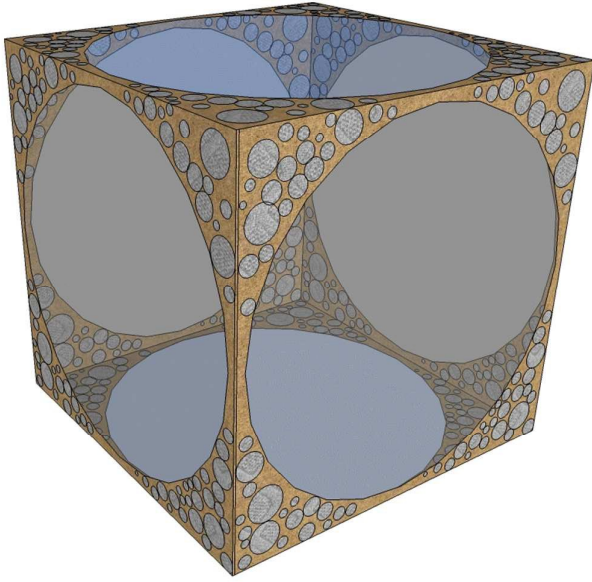


Figure 8

Bubble growth in viscoelastic dough

Turbin-Orger et al.

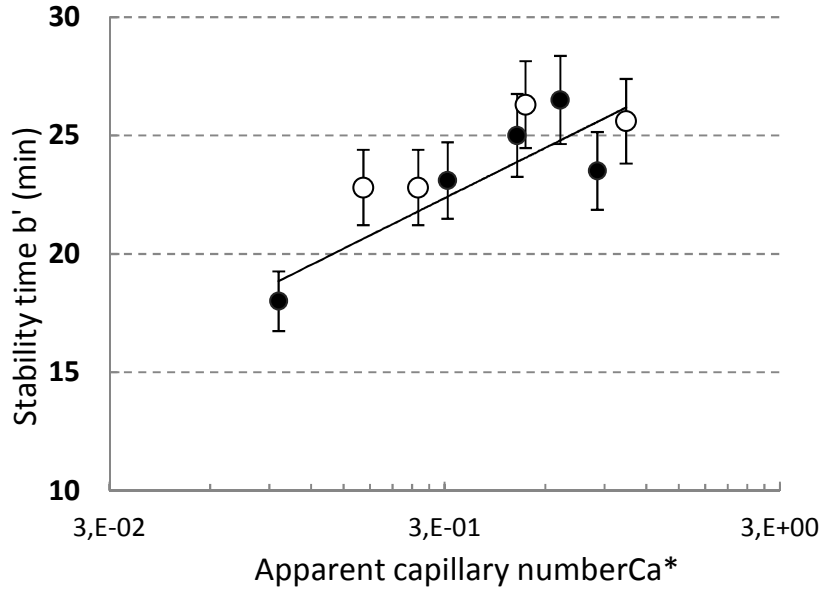


Figure 9

Bubble growth in viscoelastic dough

Turbin-Orger et al.

Table 1: Composition of dough pieces, characteristic times of fermentation kinetics determined from the 1st series of experiments, and values of connectivity index (I_{co}), mean cell size (MCS) and cell wall thickness ($MCWT$) at porosity = 0.64, determined from the 2nd series of experiments, by XRT imaging performed during fermentation, completed with stability times and elongational properties measured by Turbin-Orger³⁰.

Dough #	Water	Sugar	Fat	Φ_{vl}	Characteristic times (min)			Cellular structure features (μm) ^a			Stability time ^b	Elongational properties ^c	
					t_p	t_c	t_{wt}	I_{co}	MCS	$MCWT$	b'(min)	K(Pa.s ⁿ)	n
1	60	2	2	0.58	22	33	38	0.94	690	200	26	16.9	0.42
2	55	2	10	0.59	30	31	42	0.95	400	170	26	17.8	0.4
3	55	15	2	0.59	65	76	70	0.9	460	190	25	14.2	0.48
4	65	10	10	0.63	41	65	65	0.8	830	240	18	8.6	0.6
5 ^d	60	2	2	0.58	52	80	80	0.96	820	260	-	16.9	0.42
6	62	0	0	0.58	23	34	34	0.88	630	240	23	17.8	0.45
7	66	0	5	0.60	-	-	-	0.86	810	250	23	12.8	0.53

^a all these values were determined for yeast content 2% (2nd series), except for dough # 5

^b the stability time is defined in eq.(7).

^c coefficients of power law for elongational viscosity (eq. 6) . These values have been measured for $\epsilon_b = 1$

^d same composition as # 1 but with 1.5% yeast instead of 3% in 1st series.